INORGANIC CHEMISTRY FRONTIERS

RESEARCH ARTICLE

View Article Online
View Journal | View Issue

Cite this: *Inorg. Chem. Front.*, 2025, **12**, 5792

Linker-cluster cooperativity in confinement of proline-functionalized Zr-based metal–organic frameworks and its effect on the organocatalytic aldol reaction†

Zarfishan Dilruba,‡[a] Ardeshir D. Yeganeh, ‡[b] Sofia Kolin,[c] Sadia Noor, [a] Hassan Shatla, [b] Carl Wieland,[a] Bo-Hung Yu,[a] Katrin Gugeler,[d] Anna Zens,[a] Johannes Kästner, [d] Deven P. Estes, [e] Kristyna Pluhackova, *[c] Simon Krause *[b] and Sabine Laschat *[a]

Received 29th October 2024,
Accepted 17th April 2025

DOI: 10.1039/d4qi02724h

rsc.li/frontiers-inorganic

Metal organic frameworks (MOFs) provide unique opportunities for molecular heterogeneous catalysis by mimicking the active sites of enzymes. However, understanding and controlling the interaction between the metal node and the organic linker carrying the catalytic unit and the resulting confinement effects remain challenging. Here, in a combined theoretical and experimental approach, Zr-UiO-67-MOFs with *ortho*-*N*-acylproline-functionalized biphenyl-dicarboxylate linkers were prepared and compared with the corresponding MOFs with regioisomeric *meta*-linkers. As benchmark catalysis, the organocatalytic aldol reaction of *p*-nitrobenzaldehyde and cyclohexanone was studied. Experimental results revealed that the *ortho*-linker accelerated the aldol reactions, whereas the regioisomeric *meta*-linker decreased the reaction rate, which was rationalized by pore blocking of the *meta*-linker *via* molecular dynamics simulations. Moreover, the acid modulator used in the MOF preparation also played a critical role in the formation of acetal byproducts through competing acid catalysis. Our study provides novel insights into the cooperative catalysis between the linker-attached organocatalyst and the MOF metal center.

Introduction

Defined spatial co-arrangement of active sites inside defined confined space is a critical feature of the catalytic activity and selectivity in enzymes. Metal–organic frameworks (MOFs) are porous crystalline solids consisting of organic linkers and inorganic nodes of various geometries, which determine the structure, pore size, and topology of the crystal lattice.[1–3] By changing the size of the linkers while keeping the nodes constant, a series of isoreticular MOFs can be prepared.[1,4,5] The high porosity, structural tailorability and controllable properties render MOFs as particularly attractive materials for molecular heterogeneous catalysis which may allow to mimic sophisticated microenvironments compared to enzymes.[6,7] The catalytically active sites can be introduced into the nanoporous framework either as part of the building blocks, by post-synthetic covalent attachment to the linker, or by coordination onto unsaturated coordination site of the inorganic node.[8,9] Due to the long-range order and nanoporosity, the chemical environment of individual active sites is, in theory, well defined and comparable throughout the whole crystal. Keeping in mind that the size compatibility of the substrates and the framework enabling the reactants to access the MOF-encapsulated catalysts and products to escape from them, MOFs enable heterogeneous molecular catalysis under confinement carrying a great potential for enhanced selectivity and activity. Given its hybrid nature, the incorporation of organocatalysts in MOFs has been targeted in the past.[3,10,11]

In these first studies, the linker lengths, solvent, presence of defects and bulky functional groups, as well as the presence of coordination sites of the inorganic node in close proximity of the organocatalyst have been shown to influence the conversion, diastereo- and enantioselectivity.[12] For example, seminal work has been published on organocatalytic

[a]*Institut für Organische Chemie, Universität Stuttgart, Pfaffenwaldring 55, D-70569 Stuttgart, Germany. E-mail: sabine.laschat@oc.uni-stuttgart.de*
[b]*Nanochemistry Department, Max Planck Institute for Solid State Research, Heisenbergstr. 1, D-70569 Stuttgart, Germany. E-mail: s.krause@fkf.mpg.de*
[c]*Stuttgart Center for Simulation Science (SC SimTech), Cluster of Excellence EXC 2075 SimTech, Universität Stuttgart, Universitätsstr. 32, D-70569 Stuttgart, Germany. E-mail: kristyna.pluhackova@simtech.uni-stuttgart.de*
[d]*Institut für Theoretische Chemie, Universität Stuttgart, Pfaffenwaldring 55, D-70569 Stuttgart, Germany*
[e]*Institut für Technische Chemie, Universität Stuttgart, Pfaffenwaldring 55, D-70569 Stuttgart, Germany*

†Electronic supplementary information (ESI) available. See DOI: https://doi.org/10.1039/d4qi02724h

‡These co-authors contributed equally to this work.

aldol additions[13] with proline-functionalized MOFs,[12,14,15] in which L-proline or derivatives were either directly attached to the linker pre- or postsynthetically (*e.g.* IRMOF-10,[12a] UiO-67,[16a,b] MUF-77 [12e]) or coordinated to the metal node (*e.g.* DUT-67, H_2N-MIL-101,[12d] MIL-101(Cr), CUP-1).[17] In particular the latter is interesting for Zr-based MOFs in which modulators (monocarboxylic acids) are used to control the crystallization process, but are also incorporated as capping agents to produce low-connective metal nodes and structural defects (missing linker, missing cluster). The study on organocatalytic activity of DUT-67 utilized this aspect by incorporating L-proline as a capping agent on an 8-connective Zr-cluster.[12f] Organocatalytic studies showed a cooperative effect between the Lewis acid sites of the Zr-node and the active organocatalytic site of L-proline. However, in this approach the presence of other modulators (TFA, acetic acid) as well as the ill-defined distribution and dynamic attachment/detachment of molecular proline *via* reversible coordination chemistry results in a complex active site environment and difficult interpretation of the actual catalytic mechanism and mixed effects on selectivity. This is in stark contrast to MOFs in which proline is covalently attached (*e.g. via* amide formation) to the linker backbone and spatially fixed within the whole crystal lattice.

Interestingly, the majority of proline-functionalized MOFs are based on biphenyldicarboxylate linkers for which so far only the *meta*-proline amide-functionalized linkers were studied (Schemes 1 and 2). Using this linker geometry, the

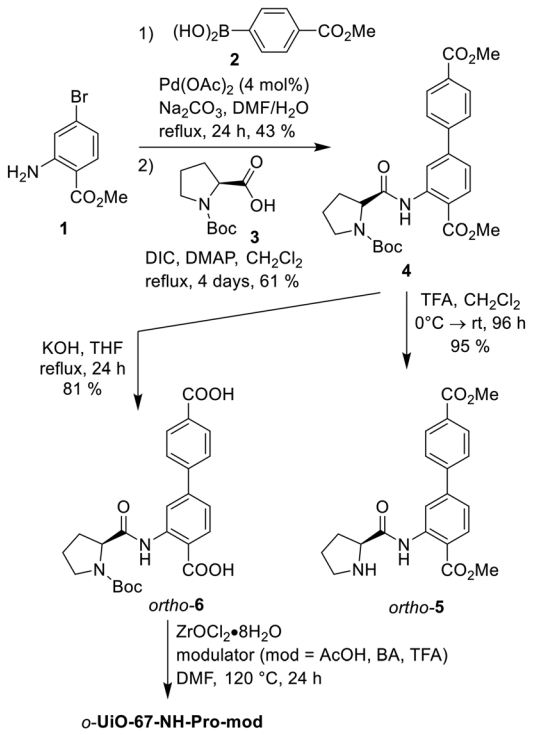

Scheme 2 Synthesis of new proline-functionalized linker *ortho*-**5** and Zr-MOF ***o*-UiO-67-NH-Pro-mod**.

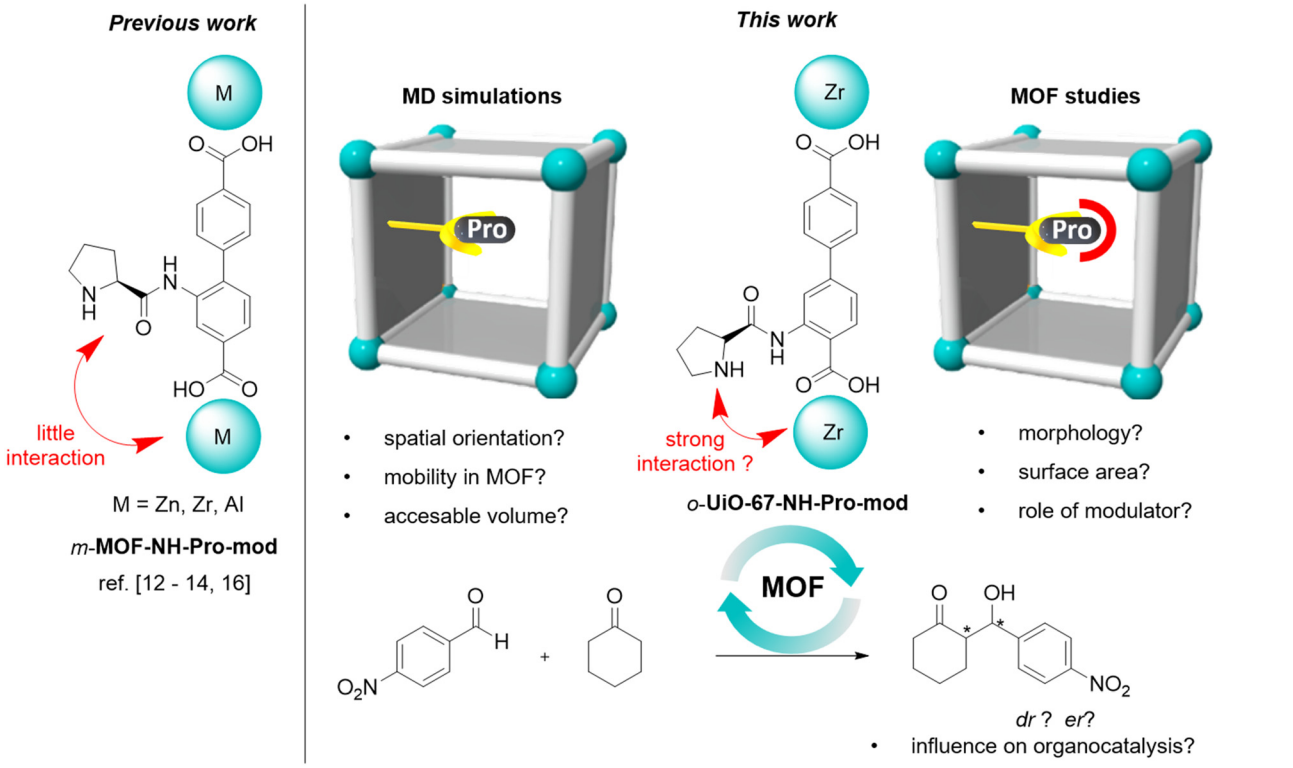

Scheme 1 Comparison of ***o*-UiO-67-NH-Pro-mod** with the known MOFs with *meta* functionalized linker.

proline points inwards the respective pores and is spatially isolated from the inorganic nodes.[12] We anticipate that MOFs with a proline function in *ortho*-position to the framework forming carboxylate and consequently in close proximity to the inorganic node might influence the organocatalysis by cooperative interaction with the metal node while still covalently fixating the proline within the framework for a defined confined microenvironment. Such cooperativity effects between catalytically active sites and support surfaces are very poorly understood, but have the potential to both hinder or enhance catalysis.[12g,18–21] Nießing *et al.* previously demonstrated such cooperativity between the metal node and the proline active site, proposing that electrophile activation can influence enantioselectivity. Their findings indicate that aldehyde coordination occurs at a distant metal center rather than the one adjacent to the proline substituent due to ring strain[12d]. Being able to control the distance between the metal node and the organocatalyst *via* substitution changes to the organic linker in MOFs has the potential to yield unprecedented insights into the role of the interaction between catalysts and supports.

In this work, we detail the synthesis and characterization of **UiO-67** derivatives based on *ortho*- and *meta*-proline amide biphenyldibenzoate linkers and investigate their performance in heterogeneous asymmetric organocatalytic aldol reactions. We identify that next to the proline position on the linker also the nature and concentration of the modulator used in the synthesis as well as the solvent used in the organocatalytic reactions have strong effects on structural features, selectivity, and activity of the catalyst. Moreover, we detail how the morphology, surface area and modulator used in the MOF synthesis takes on an active role in acetal formation as competing side reaction. Additionally, molecular dynamics (MD) simulations are performed to study the spatial orientation of the proline catalysts and the mobility of guest molecules and accessible volume in the MOFs. These properties play a critical role for catalytic efficiency, as they can determine the accessibility of reactants to catalytic sites and ensure that products can be removed promptly (Scheme 1).

Results and discussion

In order to characterize the impact of proline position relative to the metal center in **UiO-67** on the catalysis of the aldol reaction we first synthesized the respective proline amide functionalized benzoate linkers.

Synthesis of organic proline-functionalized linker

As outlined in Scheme 2 the synthesis of *ortho*-proline-functionalized linker and soluble catalyst commenced with the Suzuki coupling of methyl 2-amino-4-bromo-benzoate **1** and boronic acid **2** in the presence of 4 mol% of $Pd(OAc)_2$, followed by condensation of *N*-Boc-proline **3** with diisopropylcarbodiimide (DIC) and *N*,*N*-Dimethylpyridin-4-amin (DMAP) to give the *N*-Boc-protected dimethylester **4** in 61% overall yield over 2 steps. Deprotection of the *N*-Boc group with TFA yielded the diester *ortho*-**5** suitable for homogeneous reference catalysis. Saponification of **4** with KOH in THF gave the *N*-Boc-protected linker *ortho*-**6**.

Synthesis and characterization of proline-functionalized UiO-67 MOFs

The synthesis of proline-functionalized **UiO-67**-type MOFs (visualized in Fig. 1) follows the procedures previously published by using the Boc-protected linkers *ortho*-**6** and *meta*-**6**, respectively, to prevent side reactions of non-protected proline.[16a] In previous reports, it was found that upon solvothermal synthesis of *meta*-**6** with benzoic acid in DMF at 120 °C for 4 days, the Boc group was thermally cleaved during the MOF synthesis, liberating the catalytically active secondary amine.

To study the influence of the modulator on the deprotection, framework crystallization, and ultimately catalytic activity we synthesized ***o*-UiO-67-Pro** by solvothermal synthesis in DMF with TFA (120 °C, 24 h, further denoted to as ***o*-UiO-67-NH-Pro-TFA**), BA (120 °C, 96 h, further denoted to as ***o*-UiO-67-NH-Pro-BA**),[16a] AcOH (120 °C, 96 h, further denoted to as ***o*-UiO-67-NH-Pro-AcOH**). The same reaction procedures were carried out using *meta*-**6** as the organic linker and resulted in the MOFs further denoted to as ***m*-UiO-67-NH-Pro-TFA**, ***m*-UiO-67-NH-Pro-BA**, ***m*-UiO-67-NH-Pro-AcOH**. In addition, we synthesized **UiO-67** with the three modulators as a non-functionalized reference, further denoted as **UiO-67-TFA**, **UiO-67-BA**, and **UiO-67-AcOH**. For all reactions, a white microcrystalline powder was obtained that was washed with fresh DMF (3 times over 2 days), suspended and washed in acetone (5 times over 2 days), and dried in dynamic vacuum for at least 16 h ($<3 \times 10^{-3}$ kPa, 80 °C).

The structure and phase purity of the samples was evaluated by PXRD on as made, and dried samples. As shown in Fig. 2, the PXRD patterns for both functionalized and non-functionalized MOF samples, synthesized using all three modulators, align with the predicted powder pattern for **UiO-67**.[12c,h]

Following the specified washing and drying procedures, the reflections observed in some *ortho* and *meta* proline-functionalized samples became broader, suggesting a potential reduction in crystallinity and/or long-range order. Nonetheless, the samples showed improved crystallinity upon re-immersion in the reaction solution, indicating that these materials maintain their long-range order under the reaction conditions (details can also be seen in Fig. S1–S3†).

The Boc-deprotection during synthesis was examined by analyzing the ^{1}H NMR spectra of the digested samples in a $NaOH/D_2O$ solution.[22] Both *ortho*- and *meta*-proline functionalized **UiO-67** samples, synthesized with TFA as a modulator, underwent *in situ* Boc deprotection within 24 h, as indicated by the disappearance of the methyl peaks associated with the Boc at the chemical shift of around 1 and 1.2 ppm for ***o*-UiO-67-NH-Pro-TFA** and 1.2 ppm for ***m*-UiO-67-NH-Pro-TFA** (Fig. S7–S9†). In contrast, the *ortho*- and *meta*-proline functionalized MOFs synthesized with BA and AcOH as modulators

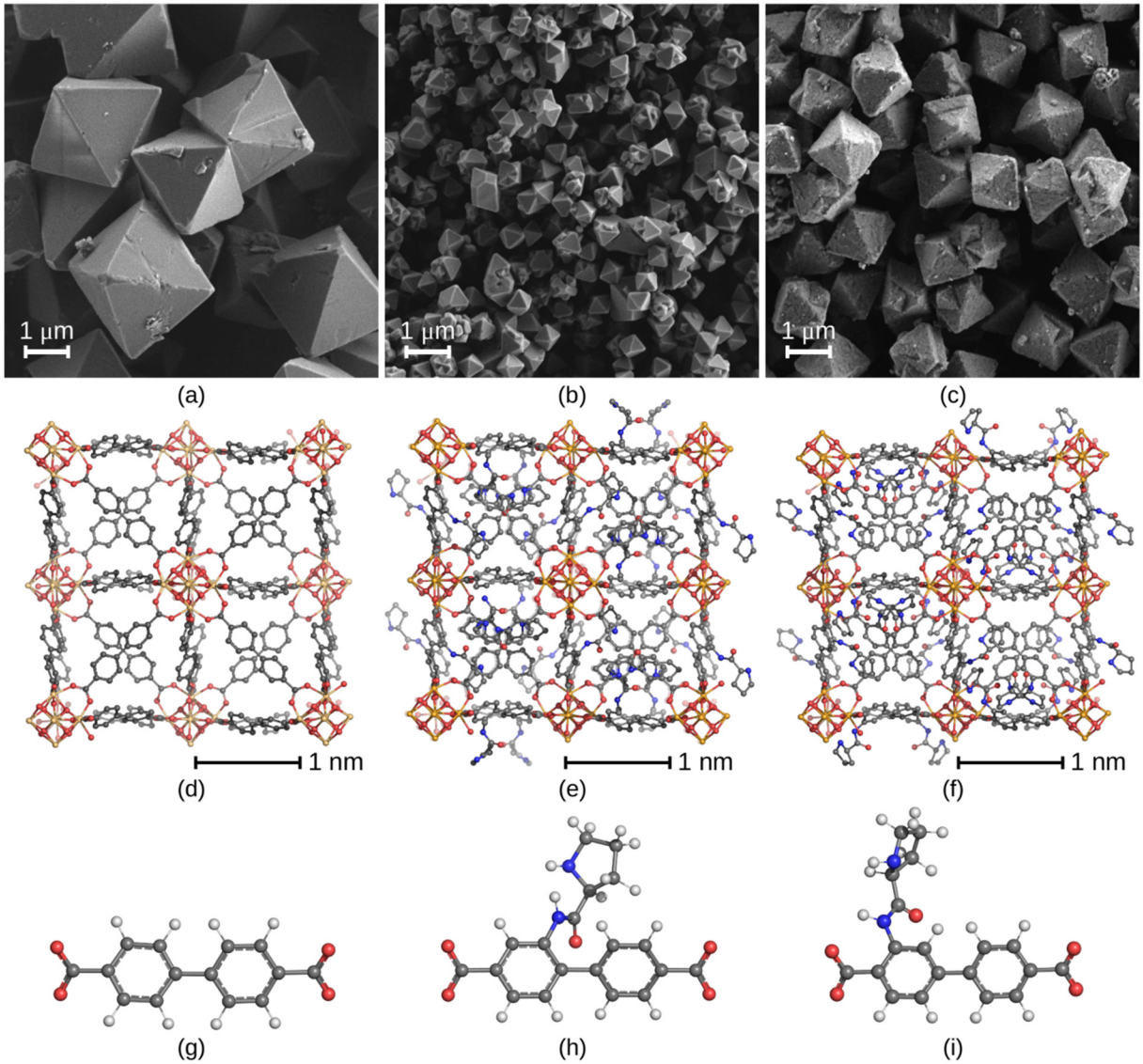

Fig. 1 UiO-67 and UiO-67-NH-Pro structures synthesized and studied in this work. SEM pictures of UiO-67 (a), *m*-UiO-67-NH-Pro (b) and *o*-UiO-67-NH-Pro (c) generated with the acetic acid modulator. The respective molecular representations of one defect-free unit cell (d–f), and the individual linkers (g–i). In the experimental structure of UiO-67 all linkers were manually substituted for proline-modified linkers with proline in position *meta* or *ortho* to obtain *m*-UiO-67-NH-Pro and *o*-UiO-67-NH-Pro, respectively.[16c] For visualization of UiO-67 type MOFs with defects, see ESI Fig. S22.† Oxygen atoms are shown in red, nitrogen atoms in blue, zirconium atoms in yellow and carbon atoms in grey. Hydrogen atoms are white in the bottom row but omitted for clarity in the unit cell representation.

showed partial Boc deprotection (80 to 96% deprotection estimated from ^{1}H NMR), after an extended reaction time of 4 days (Fig. S10 and S11†).

Previous research by Kutzscher *et al.*[16a] highlighted the key role of the strong Lewis acidity of Zr^{4+} ions in facilitating the *in situ* Boc deprotection of proline, typically requiring a reaction time of 96 h. However, our observations showed a significant acceleration of Boc deprotection when TFA as a much stronger Brønsted acid was used as a modulator, reducing the time for complete deprotection to only 24 h.

Given these findings, we proceeded with a thermal post-synthetic Boc deprotection treatment,[12a] which involved placing the MOF samples in a microwave vial containing DMF and heating them at 180 °C for 3 h. The effectiveness of this treatment was confirmed by ^{1}H NMR spectroscopy, as indicated by the absence of peaks corresponding to the Boc group post-treatment, as illustrated in Fig. S7–S9.† The ^{1}H NMR analysis of digested samples also allows us to evaluate the presence of modulators in the MOF samples. Indeed, we observe the presence of all three types of modulators in all three MOF systems in different concentrations (see Table S1†). Given that the concentrations of the modulators in the MOFs are in a comparable range, we expect a comparable impact on the catalysis. In the solid framework, these modulators act as capping ligands at

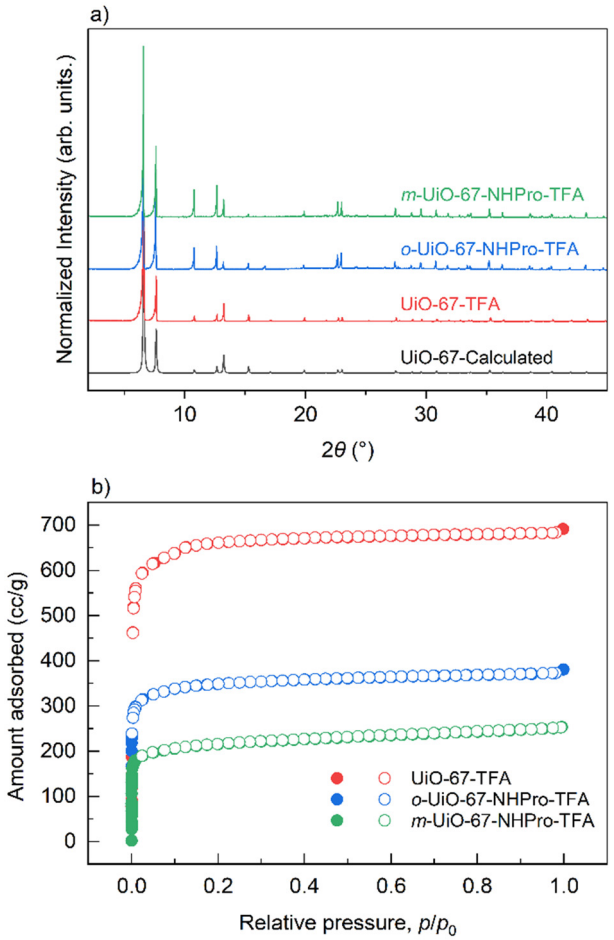

Fig. 2 (a) PXRD patterns of the as-made MOF samples with TFA as modulator; (b) nitrogen adsorption of as-made MOF samples with TFA as modulator (filled circles) and desorption (empty circles) isotherms at 77 K.

the clusters, resulting in missing linker defects,[23] that can give additional access to Lewis acid sites as well as additional nanoporosity.

We have performed thermogravimetric analysis (TGA) to obtain the chemical composition of the MOFs. Since the MOFs were dried under mild conditions and containing residual solvent and solvent decomposition products (as indicated by the H NMR spectra of the digested samples), along with the possibility of having missing cluster defects, the defect quantification using a combination of TGA and ^{1}H NMR may not have yielded a fully accurate chemical composition (Table S2†). Nevertheless, detailing the chemical composition and quantifying defects is crucial, as these factors can influence the MOF's pore structure, chemical properties, and ultimately, its catalytic performance.

We have taken SEM micrographs to analyze the morphology of the MOFs. The bare and functionalized UiO MOFs in each modulator system, have comparable crystal size and morphology within the distinct modulator system (Fig. S13–S15†). This consistency within each modulator group allows us to state that crystal size and morphology effects will play a critical factor influencing the observed differences in catalytic properties.

To evaluate the impact of the functionalization on the porosity of the samples, we recorded nitrogen adsorption isotherms at 77 K. In Fig. 2 (bottom), the MOF samples synthesized with TFA as a modulator exhibit a type-*Ib* isotherm. A decrease in nitrogen uptake is evident when proline functional groups are introduced, which can be attributed to the occupancy of the porosity with proline and a partial collapse of the framework upon solvent removal. The isotherms of the MOFs synthesized with AcOH and BA can be found in the ESI (Fig. S4 and S5†).

Homogeneous and heterogeneous catalysis

In order to compare the catalytic activity of ***o*-Ui*O*-67-NH-Pro** with the known ***m*-Ui*O*-67-NH-Pro**,[16a] the organocatalytic aldol reaction of 4-nitrobenzaldehyde **7** with cyclohexanone **8** to the *syn*- and *anti*-aldol products *syn*-**9** and *anti*-**9** was studied as benchmark reaction (Table 1).

First, the soluble proline-functionalized linkers *ortho*-**5**, *meta*-**5** were examined under homogeneous conditions. When employing a catalyst loading of 5 mol%, the aldol reaction did not go to completion even after 7 days, regardless of the tested solvent ($CDCl_3$, MeOH, DMSO). For example, *ortho*-**5** gave after 7 days in $CDCl_3$ 15% of aldol **9** with *anti*-**9** as the major diastereomer [dr (*syn*-**9**/*anti*-**9**) = 27 : 73, er *syn*-**9** = 43 : 57, *anti*-**9** = 41 : 59] and in DMSO 26% of **9** [dr (*syn*-**9**/*anti*-**9**) = 33 : 67, er *syn*-**9** = 56 : 44, *anti*-**9** = 29 : 71] (Table 1, entries 1 and 2).

In case of *meta*-**5** yields were even lower: 7% **9** [dr (*syn*-**9**/*anti*-**9**) = 38 : 62, er *syn*-**9** = 35 : 65, *anti*-*9* 9 : 91] (entry 3). However, in MeOH the acetal **10** was isolated as the major product in 40% for *ortho*-**5** (15% for *meta*-**5**), whereas the aldol products **9** were obtained only as minor byproducts (22% for *ortho*-**5**, 6% for *meta*-**5**) with similar diastereomeric and enantiomeric ratios as discussed above (entries 4 and 5). Monitoring the homogeneous catalysis in $CDCl_3$ by ^{1}H NMR over 7 days revealed a higher reaction rate for *ortho*-**5** as compared to *meta*-**5** (Fig. S9 and S10†). The reactivity difference between the regioisomers was clearly visible, when higher catalyst loadings were employed. For 20 mol% *ortho*-**5** the reaction was complete after 1 day [dr (*syn*-**9**/*anti*-**9**) = 20 : 80, er *syn*-**9** = 44 : 56, *anti*-*9* = 36 : 64], whereas 20 mol% *meta*-**5** required 3 days for completion [dr (*syn*-**9**/*anti*-**9**) = 25 : 75, er *syn*-**9** = 59 : 41, *anti*-**9** = 20 : 80] (entries 6 and 7). In general, for the homogeneous catalysis diastereoselectivities of **9** differed only little between *ortho*-**5** and *meta*-**5**. In all cases the *anti*-aldol *anti*-**9** was the major diastereomer. In contrast, with respect to the enantioselectivity *anti*-aldols *anti*-**9** possessed higher er values as compared to *syn*-aldols *syn*-**9** and er values for *ortho*-**5** were somewhat smaller than for *meta*-**5** (For further details, see Tables S4, S5 and Schemes S4–S7† for proposed mechanism).

Preliminary heterogeneous catalysis experiments with 5 mol% of ***o*-UiO-67-NH-Pro-mod** gave low yields (<12%) even after 7 days in $CDCl_3$ with both AcOH, BA or TFA modulators which did not reveal any trends (for all optimization experi-

Table 1 Homo- and heterogeneous organocatalytic aldol addition of 4-nitrobenzaldehyde **7** and cyclohexanone **8** under various conditions[16a]

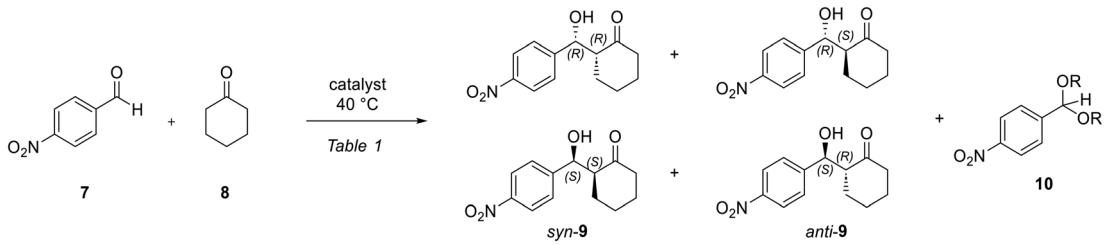

Entry	Catalyst	mol%	Time [d]	Solvent	Yield[a] **9** [%]	Yield[a] **10** [%]	**9** dr[a] *syn*/*anti*	*syn*-**9** er[b,c] *minor*/*major*	*anti*-**9** er[b] (*S*,*R*)/(*R*,*S*)
(1)	*ortho*-**5**	5	7	$CDCl_3$	15	0	27 : 73	43 : 57	41 : 59
(2)	*ortho*-**5**	5	7	DMSO	26	0	33 : 67	56 : 44	29 : 71
(3)	*meta*-**5**	5	9	$CDCl_3$	7	0	38 : 62	35 : 65	09 : 91
(4)	*ortho*-**5**	5	7	MeOH	22	40	40 : 60	59 : 41	27 : 73
(5)	*meta*-**5**	5	7	MeOH	6	15	13 : 87	43 : 57	17 : 83
(6)	*ortho*-**5**	20	1	$CDCl_3$	>99	0	20 : 80	44 : 56	36 : 64
(7)	*meta*-**5**	20	3	$CDCl_3$	>99	0	25 : 75	59 : 41	20 : 80
(8)	***o*-UiO-67-NH-Pro-TFA**	5	7	MeOH	9	9	91 : 9	42 : 58	35 : 65
(9)	***m*-UiO-67-NH-Pro-TFA**	5	7	MeOH	5	75	61 : 39	56 : 44	05 : 95
(10)	***o*-UiO-67-NH-Pro-TFA**	20	7	DMSO	59	0	79 : 21	50 : 50	50 : 50
(11)	***o*-UiO-67-NH-Pro-TFA**	20	7	$CDCl_3$	95	0	81 : 19	50 : 50	49 : 51
(12)	***m*-UiO-67-NH-Pro-TFA**	20	7	DMSO	17	0	81 : 19	50 : 50	43 : 57
(13)	***m*-UiO-67-NH-Pro-TFA**	20	7	$CDCl_3$	25	0	78 : 22	53 : 47	44 : 56
(14)	**UiO-67-TFA (0% Pro)**	20	7	$CDCl_3$	60	0	79 : 21	50 : 50	48 : 52

[a] Determined from the ^{1}H NMR spectrum of the crude product using mesitylene as the external standard. [b] Determined by HPLC on a CHIRALPAK® AD-H column, 250 × 4.6 mm, 5 μm, hexane : i-PrOH (90 : 10), 0.8 mL min^{-1}, 254 nm, 22 °C. [c] *syn*-**9**: minor (*R*,*R*) or (*S*,*S*) ; major (*R*, *R*) or (*S*,*S*).

ments on heterogeneous catalysis, see Table S6†). Use of MeOH as the solvent resulted in preferred formation of the acetal **10**, *e.g.* 5 mol% of ***o*-UiO-67-NH-Pro-TFA** gave 9% of acetal **10** and 9% aldol **9**, while ***m*-UiO-67-NH-Pro-TFA** gave 75% of **10** and only 5% **9** (entries 8 and 9). A long-term experiment utilizing 5 mol% of ***o*-UiO-67-NH-Pro-TFA** further supported this observation (Fig. S11†). When a hot filtration test was carried out after 2 days, the NMR yield of the acetal **10** increased with increasing time, while the concentration of the aldol **9** remained constant (Fig. S11b†). These results indicate that the heterogeneous catalysis takes place as anticipated only in the presence of the solid catalyst, whereas the acetal formation proceeded after removal of the solid catalyst, presumably *via* leached TFA modulator. Fortunately, at 20 mol% loading with the proline-modified Zr-MOFs containing TFA modulator the heterogeneous catalysis of the aldol addition was significantly accelerated. As shown in Table 1, entry 10, in DMSO ***o*-UiO-67-NH-Pro-TFA** gave 59% aldol **9**, preferably as the *syn*-aldol *syn*-**9** (dr 79 : 21), but racemic for both *syn*- and *anti*-diastereomers [er *syn*-**9** = 50 : 50, *anti*-**9** = 48 : 52]. Under similar conditions ***m*-UiO-67-NH-Pro-TFA** gave only 17% **9** with similar diastereoselectivity [dr (*syn*-**9**/*anti*-**9**) = 81 : 19, er *syn*-**9** = 50 : 50, *anti*-**9** = 43 : 57] (entry 12). Gratifyingly, the reactivity of the Zr-MOFs could be further improved by using $CDCl_3$ as the solvent. Thus, ***o*-UiO-67-NH-Pro-TFA** gave 95% aldol **9** [dr (*syn*-**9**/*anti*-**9**) = 81 : 19, er *syn*-**9** = 50 : 50, *anti*-**9** = 49 : 51] after 7 days (entry 11), whereas ***m*-UiO-67-NH-Pro-TFA** produced 25% aldol **9** [dr (*syn*-**9**/*anti*-**9**) = 78 : 22, er *syn*-**9** = 53 : 47, *anti*-**9** = 44 : 56] (entry 13). It should be noted, that **UiO-67-TFA (0% Pro)** (20 mol% in $CDCl_3$) was already catalytically active, yielding 60% of **9** [dr (*syn*-**9**/*anti*-**9**) = 79 : 21, er *syn*-**9** = 50 : 50, *anti*-**9** = 48 : 52] with the *syn*-**9** as major diastereomer (entry 14).

Thus, both the regioisomer of the proline-functionalized linker as well as the solvent had a major impact on the reaction rate and yields. Presumably, the reversal of the diastereoselectivity from the *anti*-preference under homogeneous conditions to the *syn*-preference under heterogeneous conditions is due to the Lewis acid catalysis taking place at the Zr nodes of the MOF in agreement with Kaskel's earlier report.[16a]

This rationale was further supported by catalytic control experiments with $ZrOCl_2{\cdot}8\ H_2O$ (15 mol%) in $CDCl_3$, which gave 5% aldol **9** albeit as an almost equimolar mixture of diastereomers [dr (*syn*-**9**/*anti*-**9**) = 55 : 45] (entry 13, Table S7†). An additional control experiment employing $ZrOCl_2{\cdot}8\ H_2O$ (15 mol%) in MeOH yielded already after 20 h 96% acetal **10** (entry 14), indicating that in MeOH the Zr-catalyzed acetalization is strongly favoured over the aldol reaction.[12a,b,e,21,24]

While MeOH accelerates the acetal formation at the expense of the aldol reaction, DMSO or $CDCl_3$ gave higher yields of the aldol product as compared to MeOH. The beneficial effect of polar solvents on the aldol reaction has been recently examined in theoretical studies by Gavali,[25] Lustosa[26] and Świderek.[27] The increased yields of $CDCl_3$ as compared to DMSO might be due to Brønsted acid catalysis accelerating both condensation step towards the iminium ion, iminium ion – enamine equilibrium, as well as final hydrolysis to

release the aldol product. On the other hand, diastereoselectivities were little affected by the solvent, presumably due to the cyclic transition states. The proposed mechanistic details of homogenous and heterogenous catalysis are depicted in Schemes S3–S5 in the ESI.†

It should be noted that the involvement of Lewis acid catalysis by the Zr nodes has also been discussed by Kaskel for UiO-66 with L-proline defect sites.[12f] The Lewis acid catalysis by the Zr node would also explain the experimental observation, that the unmodified MOF **UiO-67-TFA (0%Pro)** (Table 1, entry 14) gave a similar diastereoselectivity as compared to the proline-modified MOFs (entries 8–13). According to Kaskel the reversed diastereoselectivity might also be explained by the close proximity of the proline units from the other linker units in the MOF pore.[16a] Moreover, Telfer has emphasized that differences in the diastereomeric transition states are very small and these energetic differences are influenced by weak interactions of the catalytic intermediates with modulators and solvents.[12e]

Finally, hot filtration tests for the catalytic reactions with 20 mol% of catalysts were carried out in $CDCl_3$, which revealed that for both **UiO-67-TFA** as well as proline-modified MOFs ***o*-UiO-67-NH-Pro-TFA**, ***m*-UiO-67-NH-Pro-TFA** heterogeneous catalysis took place, *i.e.* the yield of the aldol **9** remained constant after removal of the catalyst indicating no leaching of active linkers into the reaction mixture as shown in Fig. 3.

Moreover, the following qualitative trend regarding the reaction rate was observed: ***o*-UiO-67-NH-Pro-TFA** > **UiO-67-TFA** ≥ ***m*-UiO-67-NH-Pro-TFA** (Fig. 3).

These observations indicate that the spatial orientation of the proline group within the framework plays a pivotal role in the catalytic activity and potentially other factors that may influence the heterogeneous reaction such as mass transport in the nanoporous frameworks.

Molecular dynamics simulations of proline-functionalized MOF

Consequently, the spatial orientation and arrangement of the proline groups in the **UiO-67** frameworks and its influence on the mobility of the individual molecules in the porous frameworks was studied by all-atom molecular dynamics (MD) simulations.

Our averaged MD simulations revealed markedly different spacing of the NH group on the proline catalyst and the metal centers for ***o*-UiO-67-NH-Pro** and ***m*-UiO-67-NH-Pro** (Fig. 4, top row). In detail, the NH group is most of the time 0.7–0.9 nm away from the nearest Zr in ***m*-UiO-67-NH-Pro**. In ***o*-UiO-67-NH-Pro**, on the other hand, the NH group positions itself significantly closer to the nearest Zr, namely 0.3–0.7 nm. Thus, for more than 50% of the time the proline's NH group interacts either directly with the oxygens/hydroxyl ions of the metal center or indirectly *via* methanol OH group. Similar trend is observed for the distance of the enamine "spacer" NH group and the metal center (shown in ESI Fig. S23†). Whereas the distance of 0.7–0.8 nm in the *m*-UiO-67-NH-Pro system is too large to simultaneously stabilize the aldehyde interacting with

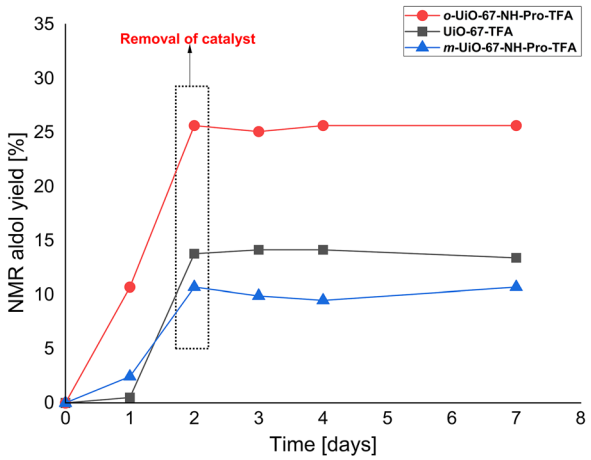

Fig. 3 Comparison of hot filtration **UiO-67-TFA**, ***o*-UiO-67-NH-Pro-TFA** and ***m*-UiO-67-NH-Pro-TFA** in the presence of 20 mol% catalyst in $CDCl_3$.

the TS3′/4′ (see Scheme S6†) by both the metal center and the spacer NH, the spacing of 0.3–0.5 nm in the *o*-UiO-67-NH-Pro is suitable for simultaneous stabilization, thus most likely improving the *syn*/*anti* selectivity of the reaction.

The drastic reduction (by 51.6% in case of ***o*-UiO-67-NH-Pro** and 58.9% in ***m*-UiO-67-NH-Pro** compared to **UiO-67**) of the accessible volume by the attachment of the catalyst on the linker is depicted in Fig. 4, bottom left. Notably, ***o*-UiO-67-NH-Pro** retains a higher accessible volume compared to ***m*-UiO-67-NH-Pro**, which suggests that the catalyst next to the metal cluster occupies less space. Fig. 4, bottom middle shows that both the presence of the catalyst inside the MOF and the catalyst's position influence the movement of methanol as a guest molecule in the pore. In agreement with the higher accessible volume of ***o*-UiO-67-NH-Pro**, methanol diffuses better in the ***o*-UiO-67-NH-Pro** compared to ***m*-UiO-67-NH-Pro**, yet the mobility is even more reduced than the accessible volume, in detail methanol travels only 29% and 22% of the average distance in ***o*-UiO-67-NH-Pro** and ***m*-UiO-67-NH-Pro** compared to **UiO-67**, respectively. The reduced mobility of methanol in ***m*-UiO-67-NH-Pro** results from the catalyst blocking the pore windows and from higher entangling of methanol with the catalyst. In ***o*-UiO-67-NH-Pro**, on the other hand, the catalyst is positioned at the outer edge of the linker, resulting in more open pore windows and thus increased methanol mobility.

Similarly, the movement of the substrates is much easier in catalyst-free **UiO-67**. Transport properties are more drastically impacted for the larger substrate and product molecules of the aldol reaction. Even though the total distance the substrates travel within 1 μs in **UiO-67** is more than ten times shorter than that of methanol, the substrates readily pass from one cage to another passing within 1 μs almost 2 unit cells (the unit cell has dimensions of $x = y = z = 2.69$ nm). The presence of the catalyst strongly restricts also the movement of the reactants. Substrate 7 reaches only 9% and 16% of the traveled

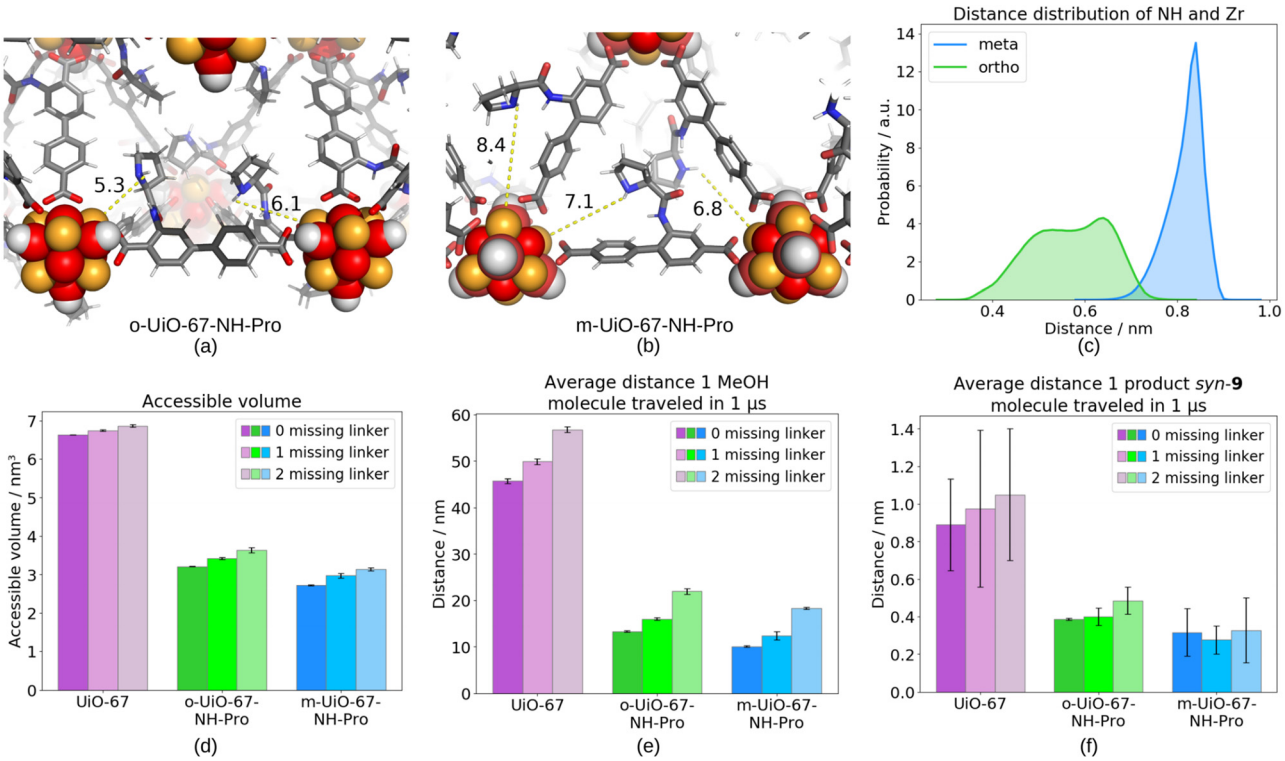

Fig. 4 Exemplary positions of the proline catalysts described by the distance of the NH-group to the nearest Zr atom in ***o*-UiO-67-NH-Pro** (a) and ***m*-UiO-67-NH-Pro** (b). Oxygen atoms are shown in red, nitrogen atoms in blue, zirconium atoms in orange, carbon atoms in gray, hydrogen atoms in white. (c) Minimal distance distributions of the NH-group of the catalyst to the Zr atom of the metal cluster in respect of catalyst position in defect-free MOFs. (d) Accessible volumes in each system. (e) Average distance that MeOH traveled in 1 μs in each system. (f) Average distance that the product *syn*-**9** covered in 1 μs in each system. The errors denote standard deviations.

distance in ***o*-UiO-67-NH-Pro** and ***m*-UiO-67-NH-Pro** compared to the catalyst-free **UiO-67**, respectively (ESI Fig. S25 and S26†). Substrate **8** is also drastically slowed down, in detail to 8% in ***o*-UiO-67-NH-Pro** and to 8% in ***m*-UiO-67-NH-Pro.** The comparably high error bars in the distances the substrates travel does not allow for distinction of the effect of the catalyst position on the mobility of the substrates in the timescale of our simulations. The situation becomes even more severe for the bicyclic *syn*-**9** product as can be seen in Fig. 4, bottom right. While the product can move slowly but steadily through the catalyst-free **UiO-67** (the average traveled distance of 0.89 nm per 1 μs corresponds to 1.4 transitions from pore to pore per 1 μs), it gets stuck in the smaller, tetrahedral pore in presence of the catalyst (0 pore to pore transitions in ***o*-UiO-67-NH-Pro** and 0.1 per 1 μs in ***m*-UiO-67-NH-Pro**). Obviously, more extensive sampling is required to ultimately analyze the product diffusion. In order to test the ability of the product to diffuse through **UiO-67** with the catalyst attached on the linker either in the *meta* or *ortho* position, additional simulations were performed at a higher temperature of 813 K. The great number of product transitions from pore to pore has enabled us to calculate average travelled distance per 1 μs, amounting to 6.89 ± 1.56 nm and 11.24 ± 2.61 nm for ***o*-UiO-67-NH-Pro** and ***m*-UiO-67-NH-Pro**, respectively. These values, being even larger that the distances the substrates travel at 313 K through catalyst-free **UiO-67**, prove the general ability of the product to diffuse through ***o*-UiO-67-NH-Pro** and ***m*-UiO-67-NH-Pro.** Yet, the slow diffusion at experimental temperature of 313 K can clearly limit the reaction efficiency by insufficient mass transport of reagents and inhibition by immobilized products. Thus, improving the mobility of the product through the MOF, *e.g.*, by utilizing a mixed linker approach or by extending the linker size or utilizing dynamic aspects of the framework, is holding a great promise for improving the **UiO-67-NH-Pro**-catalyzed aldol condensation of 4-nitrobenzaldehyde with cyclohexanone.

To estimate the role of missing linker defects, one or two linkers per simulation cell were substituted by two or four TFAs, respectively, and additional simulations have been conducted. The defect-rich MOFs show only a slight increase in the overall accessible pore volume (see Fig. 4 bottom left) but the defects systematically increase the mobility of methanol (shown as average traveled distance per 1 μs in Fig. 4 bottom middle). The removal of linkers creates additional pathways and larger pores, thus increasing methanol diffusion. However, the structural alterations introduced by missing-linker defects with TFA modulator, fail to significantly alter the mobility of substrates **7** and **8** (see ESI Fig. S25 and S26†),

as well as of the product *syn*-**9** (shown in Fig. 4 bottom right). Given that the traveled distance of the substrates and the product exhibit only minimal variation in the defective systems compared to the defect-free **UiO-67**, the steric hindrance imposed by the proline catalyst persists in restricting the overall mobility of larger molecules.

Conclusion

This study highlights how confinement and positioning of active site groups on the linker in UiO-67 MOFs influence catalysis, distinguishing it from MOF systems with lack of positional variability and further addressing the importance of understanding structure–function relationships in nanoporous MOF catalysts. As demonstrated by computational methods, by placing the proline group and its "spacer" enamine group in closer proximity to the metal clusters we achieve higher diffusivity of the molecules in the *ortho*-functionalized MOF while also providing spatial proximity of the proline and enamine "spacer" groups to the metal cluster, enabling better coordination of the transition states. We also identify the critical role of the acidic modulator in the *in situ* deprotection of the Boc group from the proline-based linker as well as their influence on the catalytic formation of acetals when reactions are carried out in methanol. We envision that our approach is viable to the construction of multifunctional active catalysts in other chemical transformations in which both Lewis acid and proline sites will act in a cooperative manner. Our extensive computational analysis indicates that linker functionalization may come at the price of reduced substrate/product mobility in the nanoporous network of MOFs and that individual missing linker defects do not alleviate this effect if substituted by TFA. The limited access of active sites in particular in the crystal interior by blocking of pore windows by the proline groups is an aspect we intend to study further also by experimental methods. To the best of our knowledge, our study is the first to consider these aspects with respect to catalytic activity in nanoporous confinement of MOFs[12d,28] and we believe this to be a critical area of research for the improved design of active molecular MOF catalysts.

Author contributions

Z.D. and S.N. synthesized the linkers and performed catalytic experiments, C.W. and B.H.Y. optimized the linker synthesis. A.D.Y. and H.Sh. synthesized and characterized the MOFs. K. G. performed DFT calculations. S.Ko. performed and analyzed MD simulations. D.P.E. provided his expertise on molecular heterogeneous catalysis. A.Z. checked the data. A.D.Y., A.Z., S. L., K.P. and S.Kr. wrote the manuscript. S.L. supervised the linker synthesis and catalytic experiments and coordinated the research. All authors proofread the manuscript and agreed to the final version.

Data availability

Data supporting this study are contained in the manuscript and ESI.† Raw data is openly available from (DaRUS) at (@sadia+ Ardi URL will be generated after publication).

Conflicts of interest

The authors declare no conflict of interest.

Acknowledgements

Generous financial support by the Deutsche Forschungsgemeinschaft (DFG, German Research Foundation) – Project-ID 358283783 – SFB 1333/2 2022, subprojects A08, B05, B08, C04, C07 and HBFG, shared instrumentation (Grant No. INST 41/897-1 FUGG for 700 MHz-NMR), the Ministerium für Wissenschaft, Forschung und Kunst des Landes Baden-Württemberg, and the Fonds der Chemischen Industrie is gratefully acknowledged. K. P. and S. Ko. acknowledge the support by the Deutsche Forschungsgemeinschaft under Germany's Excellence Strategy – EXC 2075-390740016 and by the Stuttgart Center for Simulation Science (SC SimTech). S. K. and A. D. Y. acknowledge financial support by the Carl-Zeiss-Stiftung within the NEXUS program. The authors also gratefully acknowledge the scientific support and HPC resources provided by the Erlangen National High Performance Computing Center (NHR@FAU) of the Friedrich-Alexander-Universität Erlangen-Nürnberg (FAU) under the NHR project MoTrNanoMat. NHR funding is provided by federal and Bavarian state authorities. NHR@FAU hardware is partially funded by the German Research Foundation (DFG) – 440719683. Open Access funding provided by the Max Planck Society.

References

1 O. M. Yaghi, M. O'Keeffe, N. W. Ockwig, H. K. Chae, M. Eddaoudi and J. Kim, Reticular synthesis and the design of new materials, *Nature*, 2003, **423**, 705–714.
2 H.-C. Zhou, J. R. Long and O. M. Yaghi, Introduction to metal–organic frameworks, *Chem. Rev.*, 2012, **112**, 673–674.
3 B. I. Ahmad, K. T. Keasler, E. E. Stacy, S. Meng, T. J. Hicks and P. J. Milner, MOFganic Chemistry: Challenges and Opportunities for Metal–Organic Frameworks in Synthetic Organic Chemistry, *Chem. Mater.*, 2023, **35**, 4883–4896.
4 S. Pandey, B. Demaske, O. A. Ejegbavwo, A. A. Berseneva, W. Setyawan, N. Shustova and S. R. Phillpot, Electronic structures and magnetism of Zr-, Th-, and U-based metal-organic frameworks (MOFs) by density functional theory, *Comput. Mater. Sci.*, 2020, **184**, 109903.
5 N. Stock and S. Biswas, Synthesis of metal-organic frameworks (MOFs): routes to various MOF topologies, morphologies, and composites, *Chem. Rev.*, 2012, **112**, 933–969.

6 E. B. Anderson and M. R. Buchmeiser, Catalysts immobilized on organic polymeric monolithic supports: from molecular heterogeneous catalysis to biocatalysis, *ChemCatChem*, 2012, **4**, 30–44.

7 R. Greifenstein, T. Ballweg, T. Hashem, E. Gottwald, D. Achauer, F. Kirschhöfer, M. Nusser, G. Brenner-Weiß, E. Sedghamiz and W. Wenzel, MOF–Hosted Enzymes for Continuous Flow Catalysis in Aqueous and Organic Solvents, *Angew. Chem., Int. Ed.*, 2022, **61**, e202117144.

8 J. Dai and H. Zhang, Recent advances in catalytic confinement effect within micro/meso–porous crystalline materials, *Small*, 2021, **17**, 2005334.

9 C. H. Sharp, B. C. Bukowski, H. Li, E. M. Johnson, S. Ilic, A. J. Morris, D. Gersappe, R. Q. Snurr and J. R. Morris, Nanoconfinement and mass transport in metal–organic frameworks, *Chem. Soc. Rev.*, 2021, **50**, 11530–11558.

10 X. Li, J. Wu, C. He, Q. Meng and C. Duan, Asymmetric catalysis within the chiral confined space of metal–organic architectures, *Small*, 2019, **15**, 1804770.

11 M. Lammert, M. T. Wharmby, S. Smolders, B. Bueken, A. Lieb, K. A. Lomachenko, D. De Vos and N. Stock, Cerium-based metal organic frameworks with UiO-66 architecture: synthesis, properties and redox catalytic activity, *Chem. Commun.*, 2015, **51**, 12578–12581.

12 (*a*) D. J. Lun, G. I. Waterhouse and S. G. Telfer, A general thermolabile protecting group strategy for organocatalytic metal– organic frameworks, *J. Am. Chem. Soc.*, 2011, **133**, 5806–5809; (*b*) C. Kutzscher, H. C. Hoffmann, S. Krause, U. Stoeck, I. Senkovska, E. Brunner and S. Kaskel, Proline functionalization of the mesoporous metal– organic framework DUT-32, *Inorg. Chem.*, 2015, **54**, 1003–1009; (*c*) G. Nickerl, M. Leistner, S. Helten, V. Bon, I. Senkovska and S. Kaskel, Integration of accessible secondary metal sites into MOFs for H_2S removal, *Inorg. Chem. Front.*, 2014, **1**, 325–330; (*d*) S. Nießing, C. Czekelius and C. Janiak, Immobilisation of catalytically active proline on H_2N-MIL-101 (Al) accompanied with reversal in enantioselectivity, *Catal. Commun.*, 2017, **95**, 12–15; (*e*) L. Liu, T.-Y. Zhou and S. G. Telfer, Modulating the performance of an asymmetric organocatalyst by tuning its spatial environment in a metal–organic framework, *J. Am. Chem. Soc.*, 2017, **139**, 13936–13943; (*f*) K. D. Nguyen, C. Kutzscher, S. Ehrling, I. Senkovska, V. Bon, M. de Oliveira Jr, T. Gutmann, G. Buntkowsky and S. Kaskel, Insights into the role of zirconium in proline functionalized metal-organic frameworks attaining high enantio-and diastereoselectivity, *J. Catal.*, 2019, **377**, 41–50; (*g*) G. Zhang, R. Chong, X. Zhou, J. Yang, Y. Bai, Z. H. Zhang and J. Lin, Positional Isomerism: A Novel Paradigm for Enhancing Iodine Adsorption in Functionalized Metal–Organic Frameworks, *Inorg. Chem.*, 2024, **63**, 22288–22296; (*h*) D. K. Sannes, S. Øien-Ødegaard, E. Aunan, A. Nova and U. Olsbye, Quantification of linker defects in UiO-type metal–organic frameworks, *Chem. Mater.*, 2023, **35**, 3793–3800.

13 Y. Yamashita, T. Yasukawa, W.-J. Yoo, T. Kitanosono and S. Kobayashi, Catalytic enantioselective aldol reactions, *Chem. Soc. Rev.*, 2018, **47**, 4388–4480.

14 Y. Zhang, J. Guo, J. Zhang, X. Qiu, X. Zhang, J. Han, B. Zhang, C. Long, Y. Shi and Z. Yang, Metal-organic frameworks enable regio-and stereo-selective functionalization of aldehydes and ketones, *Chem*, 2022, **8**, 1688–1704.

15 M. Zhou, E.-S. M. El-Sayed, Z. Ju, W. Wang and D. Yuan, The synthesis and applications of chiral pyrrolidine functionalized metal–organic frameworks and covalent-organic frameworks, *Inorg. Chem. Front.*, 2020, **7**, 1319–1333.

16 (*a*) C. Kutzscher, G. Nickerl, I. Senkovska, V. Bon and S. Kaskel, Proline functionalized UiO-67 and UiO-68 type metal–organic frameworks showing reversed diastereoselectivity in aldol addition reactions, *Chem. Mater.*, 2016, **28**, 2573–2580; (*b*) G. Zhang, R. Chong, X. Zhou, J. Yang, Y. Bai, Z. H. Zhang and J. Lin, Positional Isomerism: A Novel Paradigm for Enhancing Iodine Adsorption in Functionalized Metal–Organic Frameworks, *Inorg. Chem.*, 2024, **63**(46), 22288–22296; (*c*) N. Ko, J. Hong, S. Sung, K. E. Cordova, H. J. Park, J. K. Yang and J. Kim, A significant enhancement of water vapour uptake at low pressure by amine-functionalization of UiO-67, *Dalton Trans.*, 2015, **44**, 2047–2051.

17 L. Lili, Z. Xin, R. Shumin, Y. Ying, D. Xiaoping, G. Jinsen, X. Chunming and H. Jing, Catalysis by metal–organic frameworks: proline and gold functionalized MOFs for the aldol and three-component coupling reactions, *RSC Adv.*, 2014, **4**, 13093–13107.

18 S. E. Maier, O. Bunjaku, E. Kaya, M. Dyballa, W. Frey and D. P. Estes, Surface immobilized Cu-1,10-phenanthroline complexes with α-aminophosphonate groups in the 5-position as heterogenous catalysts for efficient atom-transfer radical cyclizations, *Dalton Trans.*, 2023, **52**, 8442–8448.

19 S. E. Maier, T. Nagel, M. Turan, E. Kaya, W. Frey, M. Dyballa and D. P. Estes, Comparison of the Catalytic Activity of Surface-Immobilized Copper Complexes with Phosphonate Anchoring Groups for Atom Transfer Radical Cyclizations and Additions, *Organometallics*, 2024, **43**, 233–241.

20 S. Maier, S. P. Cronin, M.-A. Vu Dinh, Z. Li, M. Dyballa, M. Nowakowski, M. Bauer and D. P. Estes, Immobilized Platinum Hydride Species as Catalysts for Olefin Isomerizations and Enyne Cycloisomerizations, *Organometallics*, 2021, **40**, 1751–1757.

21 H.-H. Nguyen, Z. Li, T. Enenkel, J. Hildebrand, M. Bauer, M. Dyballa and D. P. Estes, Probing the Interactions of Immobilized Ruthenium Dihydride Complexes with Metal Oxide Surfaces by MAS NMR: Effects on CO_2 Hydrogenation, *J. Phys. Chem. C*, 2021, **125**, 14627–14635.

22 G. C. Shearer, S. Chavan, S. Bordiga, S. Svelle, U. Olsbye and K. P. Lillerud, Defect engineering: tuning the porosity and composition of the metal–organic framework UiO-66 via modulated synthesis, *Chem. Mater.*, 2016, **28**, 3749–3761.

23 L. Liu, Z. Chen, J. Wang, D. Zhang, Y. Zhu, S. Ling, K.-W. Huang, Y. Belmabkhout, K. Adil and Y. Zhang,

Imaging defects and their evolution in a metal-organic framework at sub-unit-cell resolution, *Nat. Chem.*, 2019, **11**, 622–628.

24 U. S. Arrozi, H. W. Wijaya, A. Patah and Y. Permana, Efficient acetalization of benzaldehydes using UiO-66 and UiO-67: Substrates accessibility or Lewis acidity of zirconium, *Appl. Catal., A*, 2015, **506**, 77–84.

25 A. S. Gavali, P. J. Maliekal, V. A. Naik and P. M. Badani, Decoding the impact of solvents in altering the conversion rates and stereoselectivity in proline-catalyzed asymmetric aldol reaction, *Theor. Chem. Acc.*, 2024, **143**, 14, DOI: **10.1007/s00214-023-0**.

26 D. M. Lustosa, S. Barkai, I. Domb and A. Milo, Effect of Solvents on Proline Modified at the Secondary Sphere: A Multivariate Exploration, *J. Org. Chem.*, 2022, **87**, 1850–1857.

27 K. Świderek, A. R. Nödling, Y.-H. Tsai, L. Y. P. Luk and V. Moliner, Reaction mechanism of organocatalytic Michael addition of nitromethane to cinnamaldehyde: a case study on catalyst regeneration and solvent effects, *J. Phys. Chem. A*, 2018, **122**, 451–459.

28 K. Hemmer, M. Cokoja and R. A. Fischer, Exploitation of Intrinsic Confinement Effects of MOFs in Catalysis, *ChemCatChem*, 2021, **13**, 1683–1691.

